General Report TS-3A : Instrumentation in Geotechnical Engineering

Yoshinori Iwasaki
Geo Research Institute, Osaka, Japan

ABSTRACT

Sensors for geotechnical engineering are developing in the last decades. General report consists of two parts. The first part is to review recently developing technologies like MEMS (Micro Electro Mechanical Systems), GPS (Global Positioning Systems), BOTDR (Brillouin Optical Fiber Reflectometry), as well as wireless system. The second part contains the overview of the 11 papers that were submitted to the 17th ICSMGE.

Keywords : sensor, optical cable sensor, geochemical sensor, magnetic sensor, MEMS, TDR, GPS, BOTDR, Observational method

1 INTRODUCTION

In the preface to second edition of the textbook on Soil mechanics by Terzaghi and Peck in 1967, Prof. Ralph B. Peck added a new chapter on Performance Observation. This chapter 12 was intended to aid the engineer in the use of observational method which is at the very heart of successful application of soil mechanics. Among several good reasons to adapt observation, Dr. Peck indicates that field observations can be used for providing field performance that may be compared with some theoretical prediction and the original design could be modify to improve the initial design.

The third edition of the book by Terzaghi, Peck, and Mesri published in 1996, unfortunately, discontinued the section of "Observational Method."

This trend was the same as in the contexts of the International Conference of Soil Mechanics and Foundation Engineering. Since I was appointed as the general reporter of TS-3, I wanted to make a summary from the proceedings of ICSMGE from New Delhi 1994, Hamburg 1997, Istanbul 2001, and Osaka 2005. None of four conferences contains special lecture or session related with instrumentation except the New Delhi Conference in 1994 where a Discussion Session on "Construction, Instrumentation, and Real Time Management" was held. I attended this discussion session. The assigned chairman and the lead discusser were absent.

However, sensor instrumentation has been developing itself and several new trends are recognized today.

2 SENSORS

2.1 *Development of MEMS and geotechnical application*

MEMS are also referred to as micro-machines (in Japan), or Micro Systems Technology - MST (in Europe). MEMS are made up of components between 1 to 100 micrometers in size (i.e. 0.001 to 0.1 mm) and MEMS devices generally range in size from 20 micrometers (20 millionths of a meter) to a millimeter. They usually consist of a central unit that processes data, the microprocessor and several components that interact with the outside such as micro-sensor.

Photo-1
Biaxial Tilt Sensor
(Two sets of MEMS Tilt sensor in a perpendicular position each other)
Geokon biaxial sensor

Sellers and Taylor (2008), Geotechnical News March 2008, Bi-Tech

Photo-2 MEMS based multi points Tilt sensor
<http://www.measurandgeotechnical.com>

Proceedings of the 17th International Conference on Soil Mechanics and Geotechnical Engineering
M. Hamza et al. (Eds.)

doi:10.3233/978-1-60750-031-5-3288

Photo-1 shows a basic biaxial unit that equips two MEMS tilt sensors crossing perpendicular each other. Compare to the conventional tilt sensor, MEMS tiltsensor becomes smaller in size and less expensive as well as smaller power consumption.
SAA(ShapeAccelArray) is a commercially available multi-tiltsensor of three direction and is a rope-like array of sensors and microprocessors that fits into a small (27 mm) casing. Any deformation that moves the casing is accurately measured as a change in shape of the SAA.(Photo-2)
Not only tilt sensor, other such sensors as pressure, humidity, and temperature are become available in MEMS production.

2.2 *Geochemical Sensor*

Sakai (2001) reported significant changes of ion concentration in underground water on several unstable slopes where JR railway tracks run nearby. Geology of the slope is mudstone of young Tertiary and sliding shows creeping characteristics.

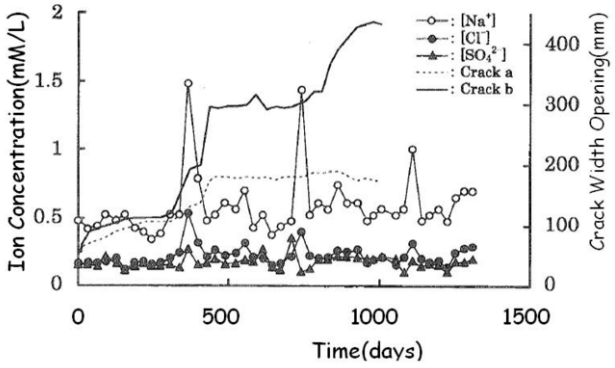

Fig.1 Change of chemical component in under ground water preceding to slope movement

On these unstable slopes, several fix points were selected to sample underground water wherefrom for study on changes of chemical components in underground water and slope displacement. The degrees of ion concentrations change with time and differ at each sampling point as well as for different ions. Based upon these sampling results, characteristic points were identified where special ion concentrations changed was preceded before sliding displacement took place.
Fig.1 shows one of the examples of such characteristic points. In this area, the characteristic ion is sodium (Na+). The determined ion concentration of 0.5 mM/L (milli moll/litter) increased to 1.5mM/L several weeks before the slope was displaced. It might be considered that leaching of ions from mud stone results in the increase of the ion concentration.

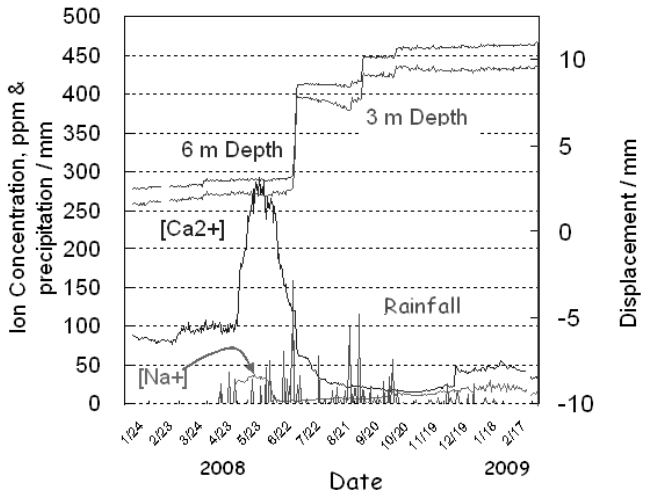

Fig.2 Chemical change with rainfall by automated monitoring

Though the precise mechanism of the sudden increase of the ion concentration is not known, the leaching causes gradual decreases of shear strength of mud stone, especially when the safety factor becomes less than unity. Increases of pore water pressure might be the direct trigger; however, monitoring of changes of ion concentration intensity is useful to provide a signal as a precursor to allow some countermeasures to be prepared.
Sakai (2009) adapted an automatic monitoring system with an ion sensor at a characteristic sampling point against the slope failure along JR railway tracks. Results of the monitoring are shown in Fig.2 where calcium ion (Ca2+) was identified as the characteristic ion rather than Na+. The increases of ion concentration were recorded about four weeks before the slop slide event that was triggered by a heavy rainfall of 160mm/day.

2.3 *Magnetic Anisotropy Sensor*

Steel shows a special characteristic of magnetization under anisotropic strain condition (*Villari* effect). If the tension stress is applied in one direction, magnetic permeability increases in the direction of the stress. If the initial value of the magnetic permeability is known, the stress change might be estimated.
Actual measurement of the magnetic permeability is rather simple to measure an induced voltage detected by sensing coils at some two points on the steel surface caused by giving magnetic excitement at other two perpendicular points from exciting coil (as shown Fig3 and Photo-3). Measurement is only to record voltage of the induced coil as a function of angle of rotation relative to the direction concerned. The voltage changes as sinusoidal function and becomes their extremes with the directions of axes of principal stresses.

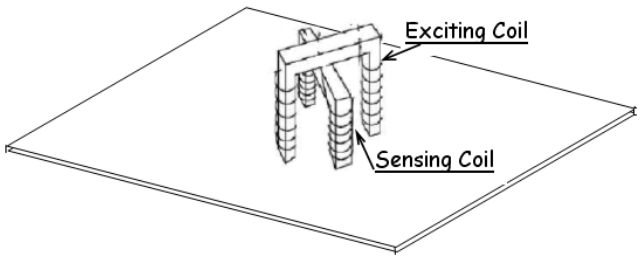

Fig.3 sensing device to detect magnetic permeability of steel plate (Sasaki, 2004)

Photo-3 Magnetic sensor

Akutagawa (2008) reported an application of this magnetic sensor to monitor the tension stress in the PS anchor to evaluate the integrity of the anchoring system in a large underground electric powerhouse cavern constructed about 10years ago. After establishing reference magnetic permeability of the steel material used in the field, the magnet anisotropy sensor was

applied to the side surface of the nut which the compression stress exists as the counter force of the tension in the PS anchor. To evaluate the anchor load after 10years operation, four PS-anchors were selected to carry out Lift off Test. For the same PS-anchors, magnetic sensor is also applied to evaluate the performance of the magnetic sensor to obtain the existing anchor load.

Table-1 Comparison among Installed Load, Liftoff and Magnetic Sensor after 10years from construction

	I.Load	Lift Off	Mag	LO−Mag	Change
	(kN)				
1	588	568	548	-20	deceased
2	588	666	656	-10	increased
3	588	515	554	39	deceased
4	588	536	511	-25	deceased

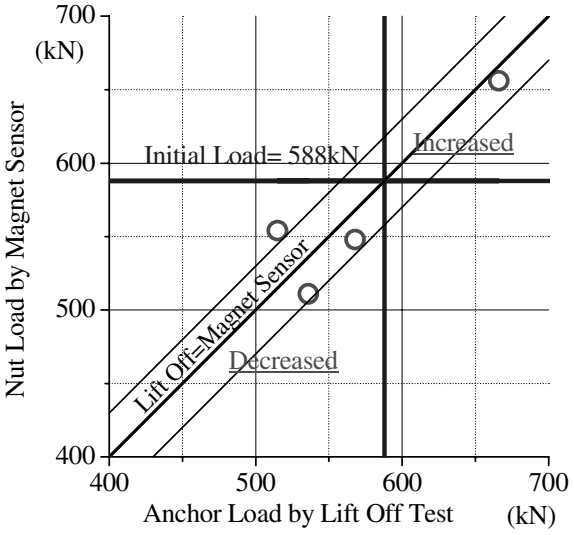

Fig.4 Load by magnet sensor and by lift off test

Table-1 and Fig.4 shows comparison of the installed load and the acting load after 10 years. The design was 588kN, the obtained values by lift off test and by magnetic anisotropy sensor are listed in the Table-1.
Among the four PS-anchors, the present load is classified into two groups of the increased or decreased from the design value. These are the same results either by Lift Off test or by magnetic sensor. The errors of magnetic sensor to the Lift off tests are -20 to 40kPa or standard deviation is 30kPa or 5% in relative to the full scale.
At present, in general, PS-anchors are left and little taken care after their installation because of no availability of appropriate feasible method. If the magnetic sensor is introduced, it will provide much easier and economical procedure to check the integrity of all of the anchors and to take any other necessary action like introducing additional load.

2.4 *Moisture Sensor TDR*

Geologists and soil scientists had recognized a relationship between the dielectric properties of soil, rock and other materials, and their moisture content. However, they lacked the instrumentation necessary to make full use of it. Time Domain Reflectometry, commonly known as TDR, largely developed as the result of World War II radar research, offered a method to define these dielectric relationships. With the advent of commercial TDR research oscilloscopes in the early 1960's, it became feasible to test this new technology. Today, TDR technology is the "cutting edge" methodology for many diverse applications including the determination of basic soil water, material/water relationships.
The velocity of electromagnetic wave in a media is known as

$$Vp = \frac{c_0}{\sqrt{\mu_s \varepsilon_s}} \quad (1)$$

where, c_0= velocity of light in vacuum($3x10^8$m/sec)
μs: specific magnetic permeability
εs: specific electric permittivity

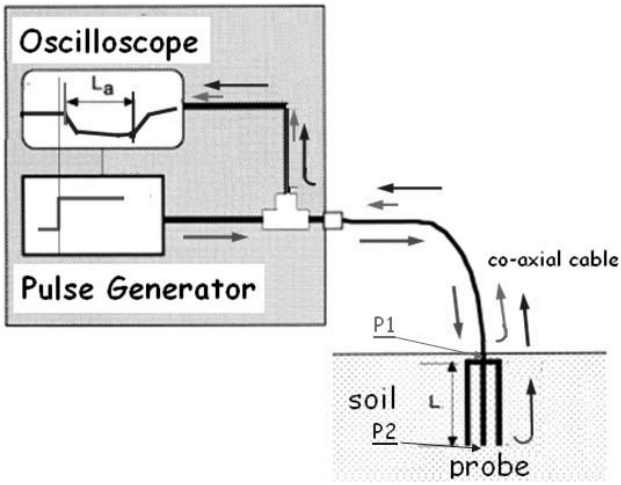

Fig.5 Basic principle of TDR Soil moisture sensor

Photo-4 MEMS based TDR moisture sensor
<http://www.decagon.com/soil_moisture/10hs/#>

In ground media, the velocity of the electromagnetic wave is controlled by permittivity of the soil components of solid particle, air, and water.
The specific permittivity of air and water is about 1.0 and 80.0. If the other component is the same, the velocity depends upon water contents of the ground.
The basic diagram of TRD is shown in Fig. 5. An electric pulse is sent from a pulse generator to the sensor via co-axial cable. When the pulse arrives at the connecting end of P1 in Fig.5 of the co-axial cable to the sensor, a small amount of energy will be reflected back and may be observed by an oscilloscope. The rest of the wave travels down to the end of the probe at P2 in Fig.5, the most of the wave energy reflects back to the co-axial cable. The reflected wave is observed in oscilloscope with a time delay of La as shown in Fig.5.
The time delay La becomes longer with larger contents of water in the ground.
The typical shape of recent TDR moisture sensor is shown Photo-4

Typical performance of the sensor is as follows,
Measure range is 0-100% in volume ratio with accuracy 2-3%.

2.5 *GPS based displacement Sensor*

GPS has been widely used to identify position on the Earth. Car navigation becomes daily use in some countries. In civil and geotechnical engineering, relative displacement is much more concern. Among several methods, Carrier phase tracking GPS provides the most accurate position information relative to the reference point at present.

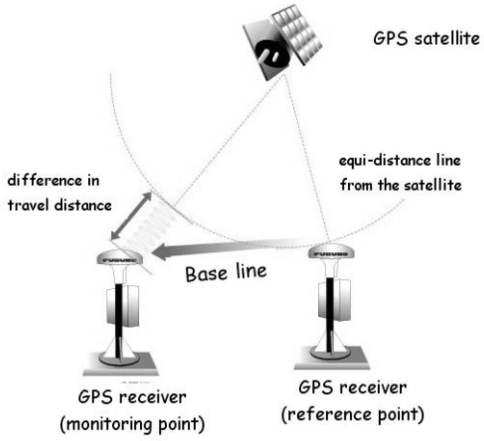

Fig.6 Carrier Phase Tracking GPS system

Carrier-phase tracking of GPS signals has resulted in a revolution in land surveying. A line of sight along the ground is no longer necessary for precise positioning.

Photo.5 GPS receiver
http://www.furuno.co.jp/product/gps/terrain/images/case_img04.jpg

Positions can be measured up to 30 km from reference point without intermediate points. This use of GPS requires specially equipped carrier tracking receivers.

Multiple points may be monitored by Carrier Phase Tracking GPS method that provides displacements relative to the reference point.
As shown in Fig.6, distance between monitoring station and GPS is divided into two segments of equi-distance and the difference. The difference in travel distance is obtained as to detect the time difference between the receiving time of the same phase of the signal carrier signals. The L1 and/or L2 carrier signals are used in carrier phase surveying. The wave length used for the system is about 19cm of the L1 carrier band.
The difference in time travel = n19 + δcm
where n is an integer number

With a 1% of wave length accuracy in detecting the leading edge, the error might be as low as 2millimiters.
Errors are caused by several factors. One of the common factors is the variation of wave velocity near the surface among the monitoring points. Wave velocity may be affected by such space conditions like humidity, temperature, and air pressure. To avoid such errors, it is better to set monitoring position with relative position within some limited range of several hundred meters.
The most time consuming process is to estimate the wave number n. Satellite is moving over the receivers from L1 to L2 along the known orbit. Using four GPS satellite signals, the phase difference as δ is obtained for every satellite. As shown in Fig.7, point P(P1 and P2) is the crossing point between ray path from satellite to the monitoring receiver and the equi-distance circle. As the satellite moves from L1 to L2, the crossing point P1 moves to P2. Since the radius of the circle is very long compared with base line, the arc from P to the reference receiver (RR) is considered as a straight line. The locus of the point P forms an elliptical orbit.

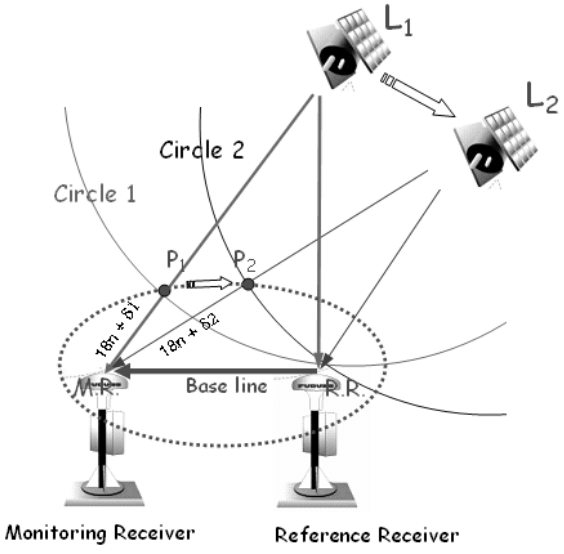

Fig.7 Determining wave number n of bias integer for Carrier-phase tracking

The wave number n is obtained as to give the minimum error to show the orbit as elliptical shape in 3D space.
A practical service system called "Shamen-net" <http://www.shamen-net.com/> provides monitoring system of Carrier Phase Tracking GPS based in Japan. The system composes from the GPS center and monitoring sites that are connected through internet. Each monitoring site consists from a local station and several GPS receivers and a reference receiver. GPS data are stored at every 30 second at the local station. The GPS data of 120 sets (60min.) is then sent to GPS center every one hour. The center shall perform analysis of the data and the results of the analyzed displacements are provided to the server at the center. The user can access and may download the monitored data from the center through internet at any place. The data is not processed in realtime at the local station. It takes about one hour from getting GPS data to see the plotted displacement graph through internet. Since the GPS system covers most of the earth surface, the system may be available in any place in the world, if internet is available. Realtime CPT GPS system may be established with additional cost at local station, if needed.
The author performed evaluation of error of the CPT GPS system that was installed in our Kobe GRI Laboratory since January 2008. The results are shown in Fig.8 that is the monitored hourly displacements for two months from February and March, 2008. The standard variations of the data are

obtained as about 2mm for horizontal and 5mm for vertical components shown in Fig.8 and Table-2.

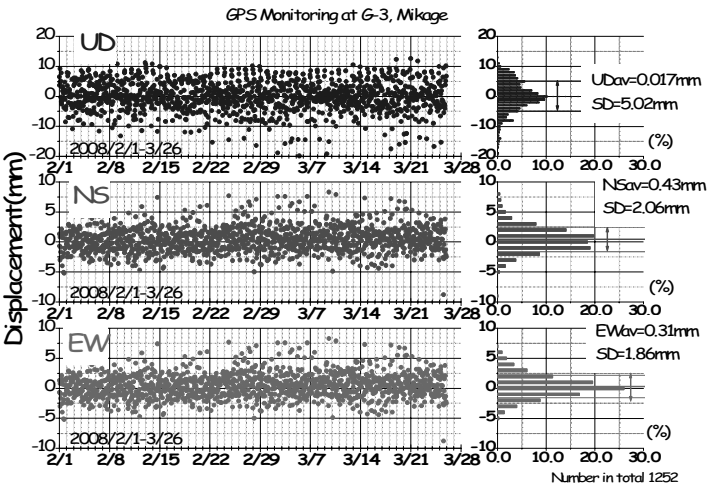

Fig.8 Distribution of observed results by CPT(Iwasaki(2008))

Table-2 Standard Deviation for three components

Component	Standard Deviation
	(mm)
UD	5.02
NS	2.06
EW	1.86

2.6 *Optical Cable Sensor BOTDR*

Fiber optics, though used extensively in the modern world, is a fairly simple and old technology. Guiding of light by refraction, the principle that makes fiber optics possible, was first demonstrated in Paris in the early 1840s. Prof. Jun-ichi Nishizawa, a Japanese scientist at Tohoku University, was the first to propose the use of optical fibers for communications in 1963. Nishizawa invented other technologies that contributed to the development of optical fiber communications. Optical fiber has been developed for sending image of medical use and for optical signal as communication cable as shown in Photo 6.

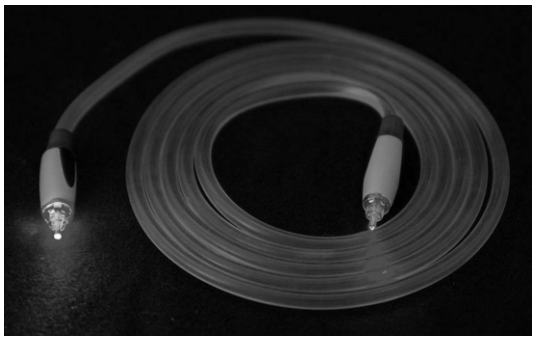

Photo.6 Optical Fiber Cable
<http;//en.wikipedia.org/wiki/optical_fiber>

Fig.9 shows a typical structure of the optical fiber that composes from core and clad. An optical fiber consists of fiber of quartz or plastics in a cylindrical shape that works as waveguide for transmitting light along its axis, by the process of total internal reflection. The fiber consists of a core surrounded by a cladding layer. To confine the optical signal in the core, the refractive index of the core must be greater than that of the cladding as shown in Fig. 10.

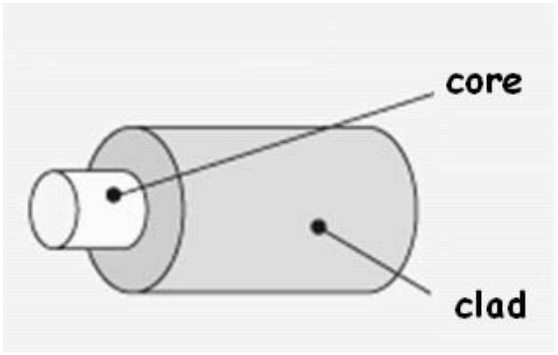

Fig 9 Basic structure of optical fiber

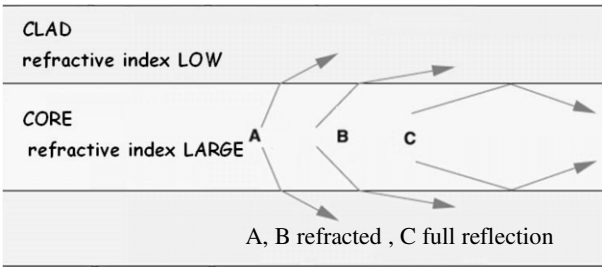

Fig.10 Full Refractive Index

The boundary between the core and cladding may either be abrupt change of refractive index, in step-index fiber, or gradual, in graded-index fiber.

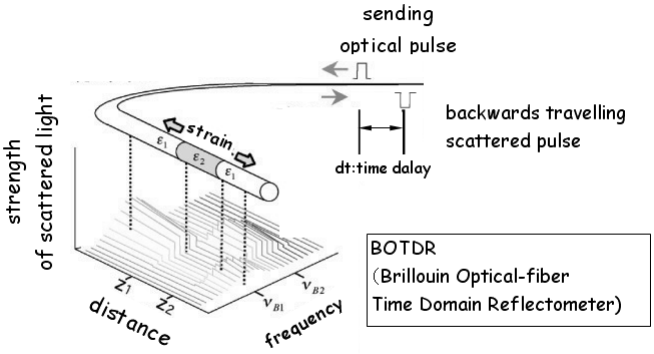

<http://www.bcm.co.jp/site/2003/2003Mar/tokubetsu-asken/tokubetsu-asken.htm>

Fig.11 Schematic Diagram of BOTDR

Single mode optical cable(SM) is designed as abrupt change to have little loss with capability of traveling long distance of 10km.

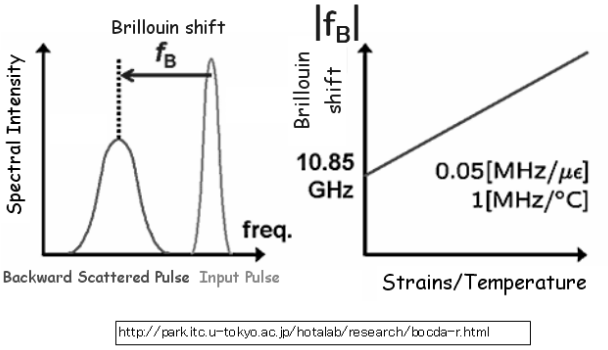

http://park.itc.u-tokyo.ac.jp/hotalab/research/bocda-r.html

Fig.12 Brillouin shift

When a sharp and strong optical pulse is sent into an optical fiber cable, some weak optical signals are returned to the entered gate as shown in Fig.11. The signals are originated from the scattering of the light at the propagating front. Backward traveling scattered light continuously arrives at the front gate. The point where the scattered signal originated is estimated by the delayed time. Three different kind of scattering are identified as Rayleigh, Raman, and Brillouin.

One of the scattered signals called Brillouin shows the frequency of the scattered pulse changes proportional to strain and temperature in the fiber as shown in Fig.12.

Since the relationship between the strain and Brillouin frequency shift is known, the analyzed frequency shift is easily transformed to the strains or temperatures. The accuracy of the measurement depends upon accuracy to analyze the value of the frequency of Brillouin shift. At present, the error range of strain is about 10-20μstrain and that of temperature is 0.5-1 degree in Celsius.

Nakano et al.(2003) reported case record of the application of the BOTDR in identifying sliding surface by inserting a pipe equipped with optical fiber in a slope as shown in Fig.13. The pipe strain gage with optical fibers gives continuous change of the strain compared to conventional pipe strain measurement. As shown in Fig.13, the strain shows continuous change from compression to extension that corresponds to bending deformation at the depth of 11m, where the sliding surface was identified.

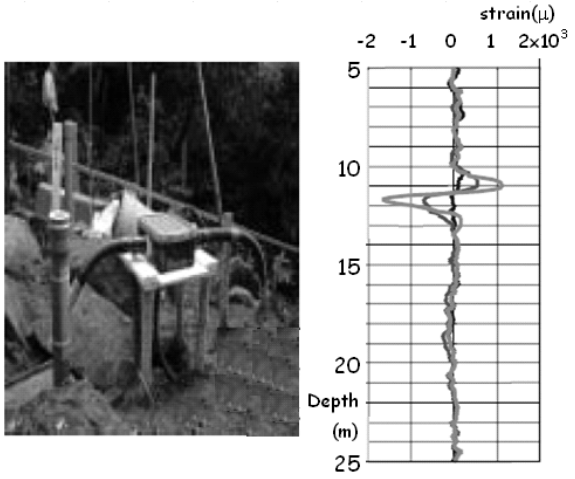

Fig.13 Detection of sliding depth by vertical pipe (by Nakano et al.,2003)

Okuno et al.(2003) applied BOTDR to monitor axial strain along the horizontal tunnel with a diameter of 3.55m for communication cable when the tunnel was to exposed to the nearby construction. As shown in Fig.14, a deep excavation along the tunnel with a short distance of about 2.4m was planned. Before excavation, a retaining wall was constructed by soil mixing pile wall (SMW). To evaluate the effects of SMW construction upon the safety of the tunnel, an optical cable for BOTDR was installed at inside surface along the spring-line at the middle of the diameter. Strains along the horizontal axis, longitudinal strains are continuously monitored. Typical example is shown in Fig.15. When the SMW construction front approached the monitored distance, strains are shifted about 40 to 80microns of compression/tension strain of within the allowable strain of 100 μ and the construction was safely completed.

Among the session TS-3, Mohamad(2009) presents case studies of optical fiber cable used to evaluate the performance of piles for building foundation and retaining wall.

Application of BOTDR may become to provide one of the most useful monitoring systems in geotechnical engineering.

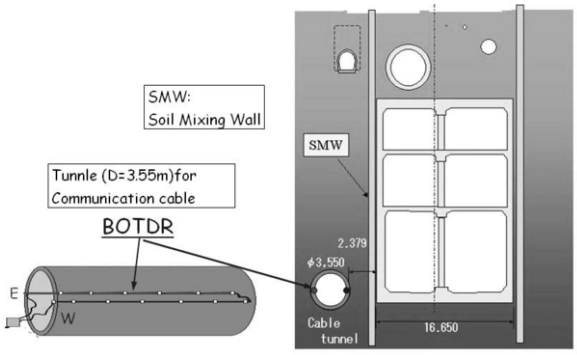

Fig.14 BOTDR along existing tunnel(Okuno,2003)

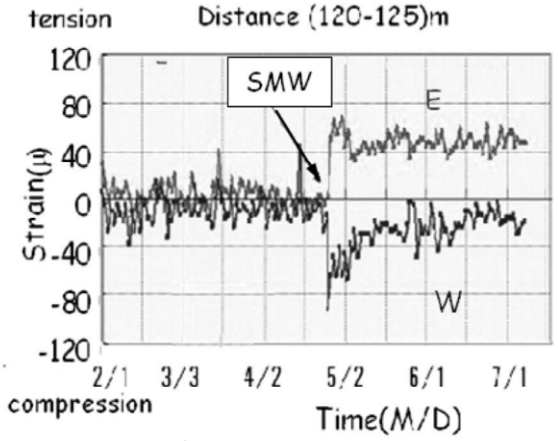

Fig.15 Strains by BOTDR of tunnel by nearby SMW

2.7 *Wireless sensor net work for monitoring*

Field monitoring system is also being advanced. One of such systems is wireless sensor net works

Wireless sensor networks represent an entirely new way of looking at computer and monitoring. In a sensor network, dozens, hundreds, or even thousands of tiny, battery-powered computers, often called “motes”, are located throughout the site to collect sensor data, e.g. strain, displacement, porewater, stress, load, temperature et al. The Motes form ad-hoc network nodes that relay the sensor data, to a specified destination for processing.

Networking diagram is shown in Fig.16 where the system consists from a Gateway and nodes.

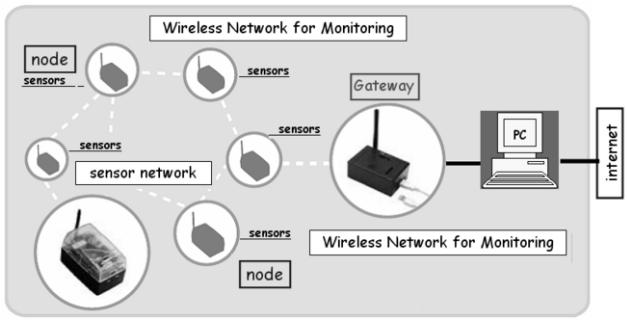

Fig.16 Wireless networking for monitoring

Each node contains tiny computer chip with sensors by MEMS, battery, and antenna for communication. Traditional way of data

logging by wireless is realized by a repeated procedure of calling a specified station by mother station and receiving the data from the station. In the wireless network system, gateway broadcasts a request to send the data to nodes and the nodes, when received the message, broadcasts the request again. The output power of wireless is limited and the broadcasting range is about a few hundred meters or even shorter because of legal regulation. The repeat broadcasting extends the monitoring range. Each node is an independent monitoring station and has a clock to control as well as built-in sensors and electric terminals to accept analog/digital signals from outside sensors.
The monitored data at each node points is stored in a file and sent back to Gateway when a request is received by the node.

Table-3 Papers presented in TS-3

Subject		First Author	Title of Paper	nation
Sensor	1	Arab, M.G.	Using MEMS based RH sensor to measure high total suction	USA
	2	Aw, E.S.	High Response Piezometer and its application at a high-speed railway site	USA
	3	Mohamad, H.	Fibre optic installation techniques for pile instrumentation	UK
Observational Method	4	Castro, J.	Field instrumentation of an embankment on stone columns	Spain
	5	Johnson, S.R.	Monitoring of mining-induced seismicity at Grassy Trail Reservoir	USA
	6	Cuellar.,V.	Improvement of transition zones for an old embankment	Spain
Slope Instability	7	Petkovsek, A.	Soil matric suction as an indicator of the mud flow	Slovenia
	8	Millis, S.W.	Real-time Monitoring of Ground Movement and Groundwater Conditions associated with Landslides in Hong Kong	HongKong
	9	Uchimura, T.	Development of low-cost early warning system of slope instability for civilian use	Japan
Reinforced Retaining Wall	10	Riccio, M.	Performance of a block-faced geogrid wall using fine-grained tropical soils	Brasil
Back Analysis	11	Hommels, A.	Influence of the different types of measurements on the inverse modelling process of an road embankment	Netherlands

3 THE REVIEW OF THE PAPERS PRESENTED

11 papers that are listed in Table-3 are presented in Technical Session 3 of instrumentation are reviewed in the following section. These papers are grouped into five categories of Sensor, Observational Method, Slope Instability, Reinforced Retaining Wall, and Back Analysis of inverse modeling problem.

3.1 *Arab, M.G. Using MEMS based RH sensor to measure high total suction USA*

Arab MG. et al. have selected a MEMS based sensor that measures not only relative humidity (R.H.) but also temperature and performed a series of calibration test against R.H.

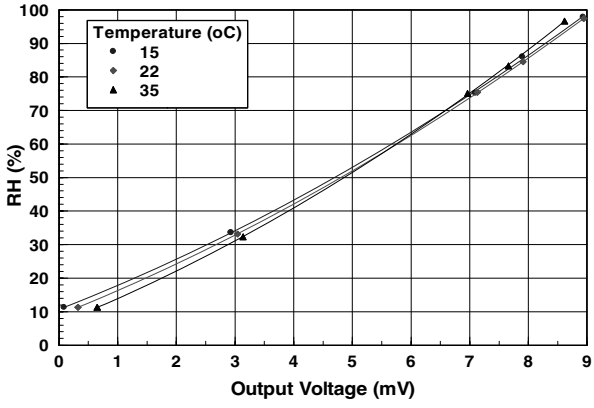

Fig.17 Calibration for the R.H. with different temperatures

It was confirmed that a MEMS based sensor is capable to measure R.H. with enough accuracy when calibration is performed for each sensor. It is well established that, if an aqueous solution of suitable concentration is enclosed inside a desiccators, the volume above the solution will equilibrate to a known relative humidity or known partial pressure of water vapor. In order to obtain different relative humidity values above the solution, several different saturated salt solutions or slurries were prepared.
Fig.17 shows output voltages of the sensor to different five R.H. with three different temperatures. Hysteresis was also studied and the errors were found within a reasonable range. Based upon calibrations performed, the MEMS based Relative Humidity sensor may be used to measure total suction in the field within a range of 3Mpa to 300MPa.
The thermodynamic relationship between soil total suction and soil relative humidity can be written as follows:

$$\psi = -\frac{RT}{M_v}\ln(RH\% * 100) \qquad (2)$$

Where ψ is the total suction of the soil, R is the ideal gas constant (8.314 J/mol-°K), T is the absolute temperature (°K), Mv is the molar volume of water (1.8×10^{5} m^3/mol), and RH is the soil relative humidity.
Two kinds of soils were used to obtain Soil-Water Characteristics Curves. The soil samples were kept in the constant R.H. in the desiccators for different 5 chemical solutions. Soil-Water Characteristic Curves obtained for the two soils are shown in Fig.18.

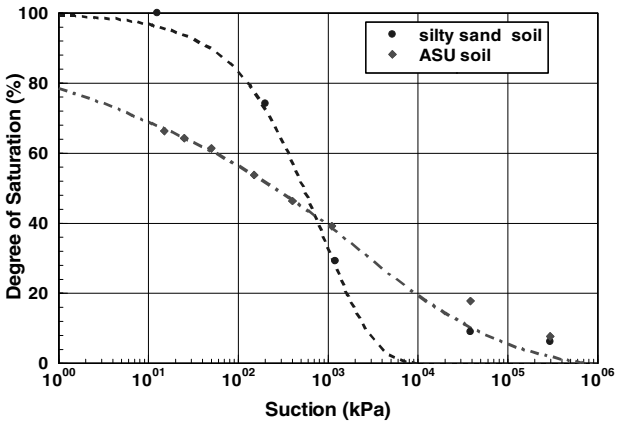

Fig.18 Soil Water Characteristic Curve

Soil-Water Characteristic Curves obtained for the two soils are shown in Fig.18. The data points were then fitted using the Fredlund and Xing fitting equation.
It is important to note that the SWCC data is shown in terms of matric suction while the relative humidity measurements are related to the total suction. The small differences between measurements obtained by the relative humidity sensor and the pressure cell are probably due to osmotic suction but further testing to validate this fact is undergoing. If the MEMS sensor becomes to provide enough accuracy to measure the suction pressure, the sensor will contribute the advancement of the study of unsaturated soils.

3.2 *Aw, E.S. High Response Piezometer and its application at a high-speed railway site, USA*

Aw., E.S. et al. describe a process of developing a low cost, miniature pore pressure sensor with a very short response time. To measure response of pore pressure in a soil under the railway tracks on which an eight carriage train runs with high speed of 150m/h. The loading duration is about 3 seconds. A commercially available pressure sensor was selected by several such reasons as long term stability, high voltage output, small and stiff diaphragm, as well as low price.
The basic sensor element is MEMS sensor with dimension of 27x28x14(mm) as shown Fig.19.

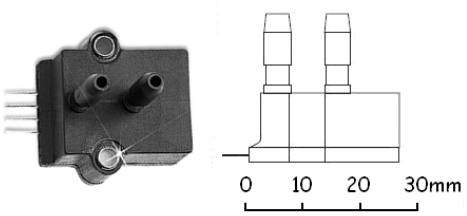

Fig.19 MEMS based pore pressure gage

The sensor system with MEMS based pore pressure sensor was developed and shown in Fig.20. A miniature steel tube with outside diameter of 3.2mm was connected to the sensor. At the end of the steel shaft, a porous filter element of 1.76mm diameter with pore size of 40microns is equipped. Silicon oil with low viscosity was used to fill up the inside of the shaft.
Based upon the compressibility and viscosity of the sensor system, the characteristic response time was calculated as 0.01sec. This value was comparable to the value of 0.04sec as experimentally obtained.

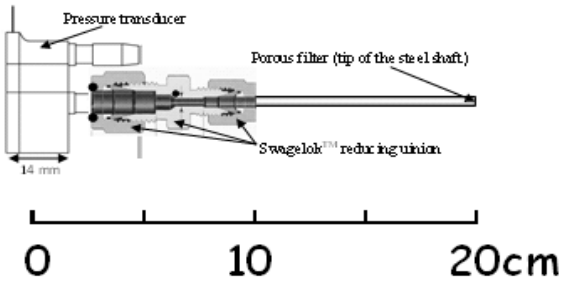

Fig, 20 Configuration of the pore pressure sensor system

The response time is governed by the compressibility of the silicone oil and the permeability of the porous filter. Laboratory tests were carried out as applying static loading for clay and sand. For clay, the response was rather slow because it is required for the water in clay to move out and flow into tube through filter. For sand, the water pressure does not fully transmitted to the sensor because sand skeleton shares some part of the applied load and dissipate very quickly due to high permeability.

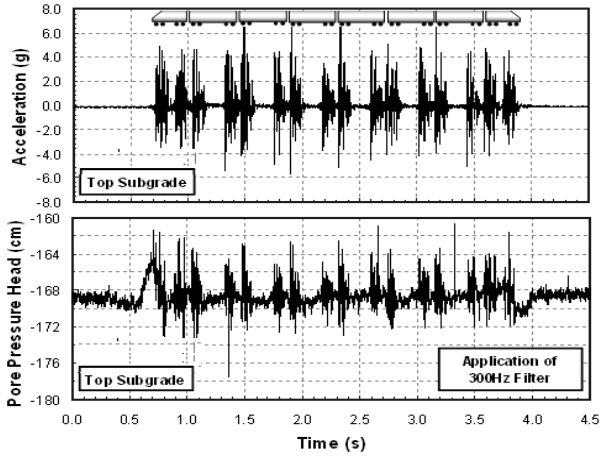

Fig.21 Typical measured acceleration and pore pressure

It should be realized the pore pressure measurement is dependent upon the mutual interaction between the permeability characteristics of soils and compressibility of the sensor system.
For the field measurement of pore pressure caused by Amtrack trains, two piezometers were installed at 0.3m in depth from the ballast surface where ground water level was about 2m below the top surface of the ballast.
Fig.21 shows typical example of response of the sensor with 10kHz sampling and post low pass filter of 300Hz. The pore pressure shows negative value of -170cm because the sensor installed above the ground water. Acceleration was also monitored near the sensor. During the passage of train, the acceleration as well as pore water pressure response for passing each wheel. However, some special responses of pore pressure are notified different from acceleration. A positive pressure increases before the train passes and some negative pressure remains after the train passes. These are static effects caused by train loading. Since the pore water is not accumulating but dissipate quickly, it was concluded that the ballast fouling may be attributed by mechanics..

3.3 *Mohamad,H., Soga,K., & Bennett, P. J.,2009, Fibre optic installation techniques for pile instrumentation, U.K.*

Mohamad et al.(2007, 2009) show some BOTDR application to monitor axial strain of bored piles and lateral deflection of retaining wall of secant pile wall of a series of intersecting reinforced concrete piles.
The diameter of the secant wall was 450mm and a pair of optical fiber cable was installed along steel cage giving a pretension of 2000μstrain. Another single optic fiber loose tubed cable was equipped along the monitored pile. Fig.22 shows how to evaluate lateral deformation from the edge strain along a pile. The edge strains are induced by mix modes of axial compression and bending deformation. To obtain bending strains, axial compression is to be separated. These axial components should be subtracted from the apparent edge strains as shown in Fig.22.
Temperature is another factor that affects upon the apparent strain values. Fig.22 shows an example of the measured strains of BOTDR for retaining wall after excavation. The excavated level was about -4.5m. Fig.22 (a) shows two edge strains of outside and nearside of the pipe as well as axial strain of the averaged values.
Fig.22 (b) shows rather constant temperature in the soil up to a level of -6.5m and gradually decreases to -13 degree at the top of the pipe.

The air temperature was lower than the in the ground, temperature decreases from near the ground surface to the top of the pile.

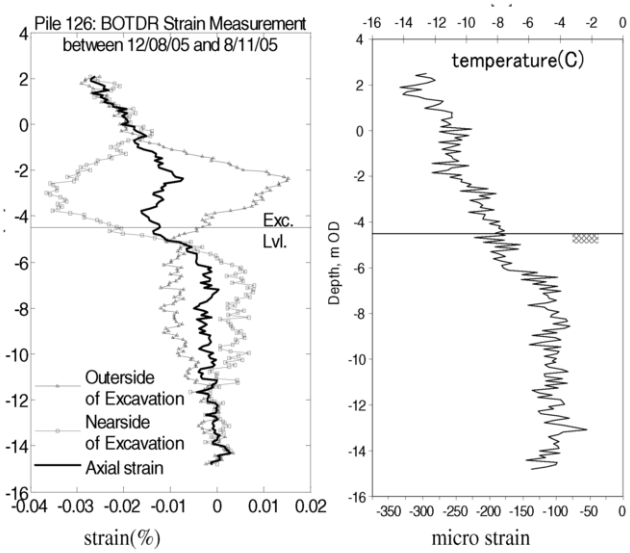

Fig.22 Strain evaluation of BOTDR equipped with secant wall

Fig.23 shows comparison between a lateral deformation curve obtained from BOTDR and two curves by conventional inclinometer measurements. It is noticed that the averaged curve of the two deflection curves from the conventional inclinometer corresponds well to the one from BOTDR.

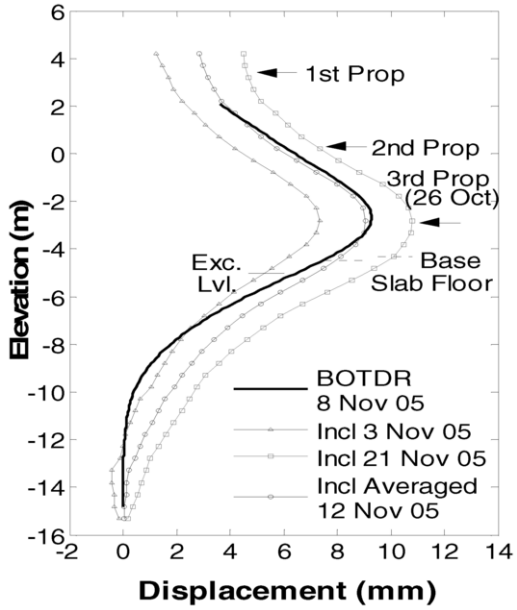

Fig. 23 Comparison of displacement by OTDR vs. Inclinometer

Compare to the conventional inclinometer of manual handling, inclinometer system by BOTDR provides automatic and realtime evaluation of deformation of retaining wall. Inclinometer measures inclination angle relative to gravity. BOTDR measures a pair of the edge strains under bending mode. It should be notice that the distance between two edges must be wide enough to keep acceptable accuracy of bending deformation.

At present, the facility to send and receive the signal as well as analyzing the BOTDR is rather expensive, In the near future, the cost effective system is expected available and become useful especially for big and deep excavation works.

3.4 *E Castro, J. Field instrumentation of an embankment on stone columns Spain*

Castro describes a case study of stone columns for soil improvement of soft ground with embankment of 10m near Valencia in Spain.

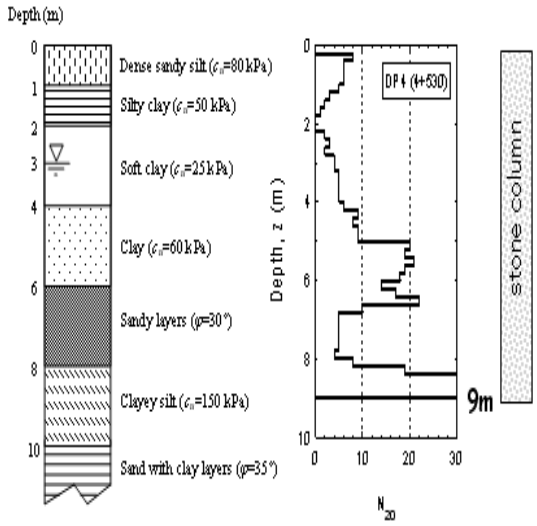

Fig.24 Geotechnical Condition

Geotechnical condition at the site is shown in Fig.24. A sensitive soft clay of 2m thick from GL-2m to -4m was anticipated to cause a large settlement. Stone column was designed to install down to the GL-9m at which bearing layer was assumed. The diameter of the column was 0.8m and installed in a diagonal shape with a distance of 2.8m.

Monitoring of stress and settlement (see Fig.25) were performed and the results were shown in Fig. 26.

The vertical stresses at the columns are several times larger than without columns. This is due to the concentration of load of embankment to the stone columns.

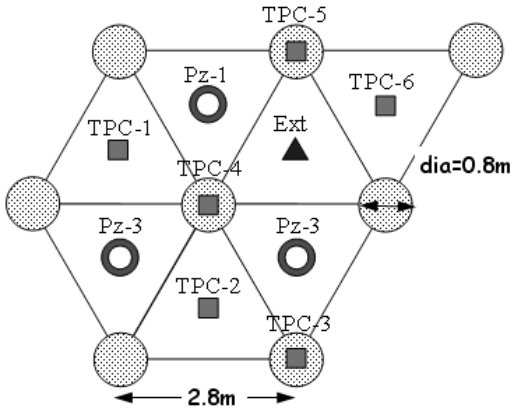

Fig.25 Instrumentation layout

However, the vertical stress at the gravel column shows only the same pressure of the embankment. This is because the sand mat layer used to protect the pressure gauge and resulted in the decrease of the stress above the gravel pile. The vertical load without the columns shows about 60kPa that is about 25% of the total embankment load of 250kPa.

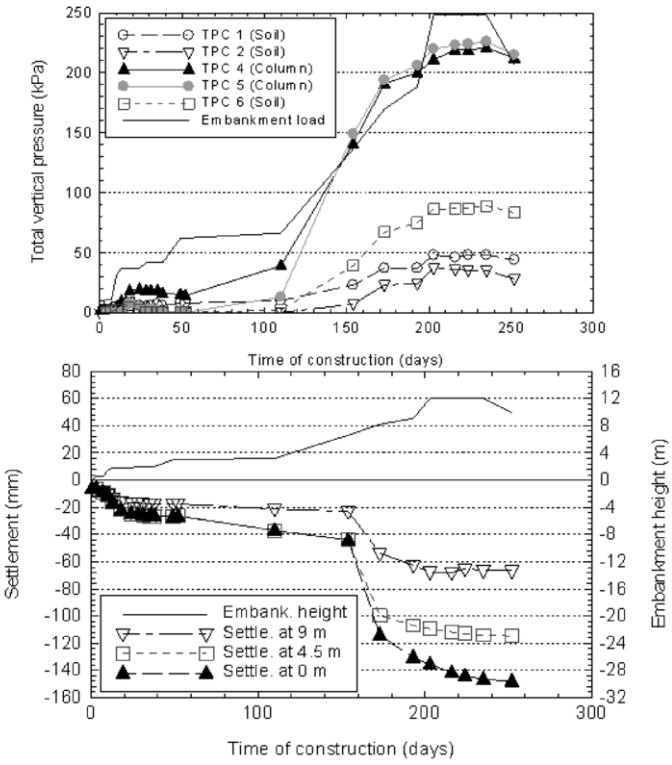

Fig.26 Time change of embankment pressure and settlement

The monitored results were confirmed by simulation of the construction process. The stone column was successful to control the settlement within the safety range by the stress concentration to the column.

3.5 *Johnson, S.R. Monitoring of mining-induced seismicity at Grassy Trail Reservoir*

Mining induced seismicity was reported as well as some deformation of the earthen dam near the mining activity. Coal mining located near the dam, 27m in height, 183m in crest length with the shortest distance of about 580m (500m in vertical and 300m in horizontal). Seismographs were installed at dam crest and hillside slope as shown in Fig.27. During a period of extraction of coal from panel 6 and 7 in 2005 an 2006, 1000 and 1500 events were recorded at the dam and hillside stations.

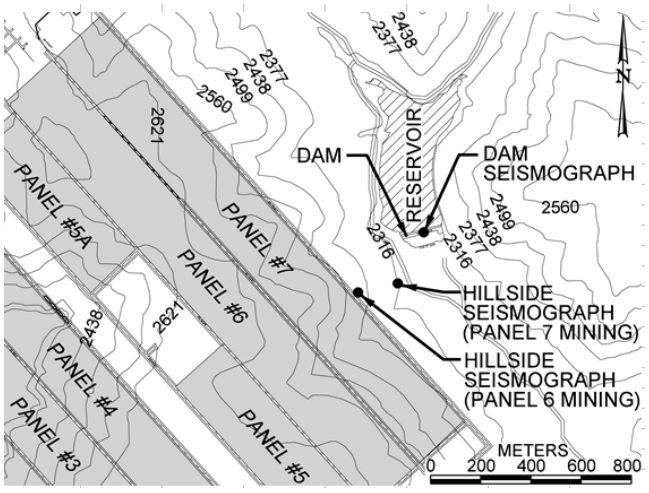

Fig.27 Site plan near the coal mining

University of Utah Seismographic Station (UUSS) recorded 300 events by UUSS network station. UUSS calculated magnitude of these events. The average magnitude is about M=1.6. Since a relationship between the magnitude and distance was established, the mining method like quantity of exclusive to be used for one blasting might be controlled.

It is further reported that the west abutment resulted in 10mm horizontal displacement. During the mining of panel 7, some survey points at hillside west of the reservoir moved eastwards 350mm with downward movement approaching 550mm.

While some deformations appeared during the mining, these movements have ceased after mining activity near the dam was complete.

3.6 *Castro, J. Field instrumentation of an embankment on stone columns Spain*

This paper reports a case study of evaluation of an embankment of 650m in length at Mantagut, Spain. There is an underpass concrete block of 8m high and wide as shown in Photo-7.

Photo-7 an underpass concrete block

The underpass point was recognized as a problem zone that required a strong limitation of very low speed of 10km/h. After several studies of geotechnical characteristics, it was decided to evaluate the embankment by monitoring vertical deflections of rail by laser technology of the accuracy of 0.01mm and the related train loads by strain gauges installed on the side surface of the rail web. Two examples of the monitored data at S2(rail track within concrete underpass) and at S3(rail track on the embankment at 45m from the underpass) is shown in Fig.28.

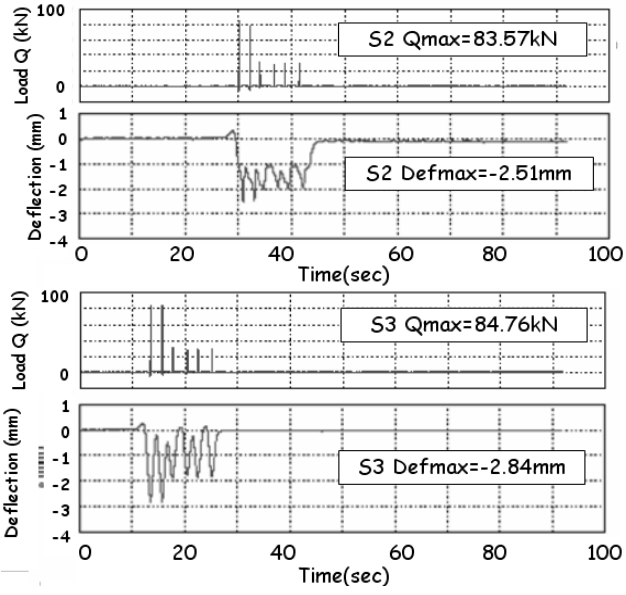

Fig.28 Load and Deflection of track caused by passage of a train

The monitored wheel loads and settlements for two points are about the same as 84kN and 2.5-2.8mm.
The deflection at the underpass point shows biased settlement during the train passing is considered due to a poor mechanical behavior of the ballast. For further study of the track stiffness K values, various types of trains were used to cover wide range of load from 20kPa to 100kPa. The embankment was divided into three sections and evaluated by the track stiffness.
The improvement of the base structure beneath the rail track was decided by replacing the embankment soil of 2.5m from the surface with well compacted sandy gravel for the embankment of 20m at both sides of the concrete block. Two layers of geogrid were used to reinforce the new material. The existing layer of 0.35m thick was replaced by high quality ballast at the top of concrete block as well as the both sides of longer than 100m.
After the improvement work, these sections were again tested and the track stiffness was evaluated and confirmed the significant increase of 2.5 to 4 times of the values of the track stiffness. The direct evaluation of the stiffness as an Index by the simple yet accurate test at the site was successful to identify the problem to be improved.

3.7 *Petkovsek, A.Soil matric suction as an indicator of the mud flow occurrence Sloveniasite, USA*

The Slano blato, which means salty mud in the Slovenia language, landslide is one of the largest and most active landslides in Slovenia. In dry season, it behaves as slow moving landslides, while in wet season, it moves as a viscous earth flow with the occurrences of rapid mudflows. Geology in the vertical section is shown as Fig.29.
The landslide is located below the contact line between Triassic limestone and Eocene Flysch formation, where spring water was found and had been regulated. Flysch formation that is sedimentary deposited in deep sea and consists of layers of marl and sandstone with thickness of a few centimeters and up to a few meters. Limestone is over- thrusted on the Flysch a very large distance and the geological structure is highly tectonized and folded. The massive and thick marly layers soften very easily and forms top formation of heterogeneous clayey gravel with blocks of Triassic limestone, sandstone and marl.

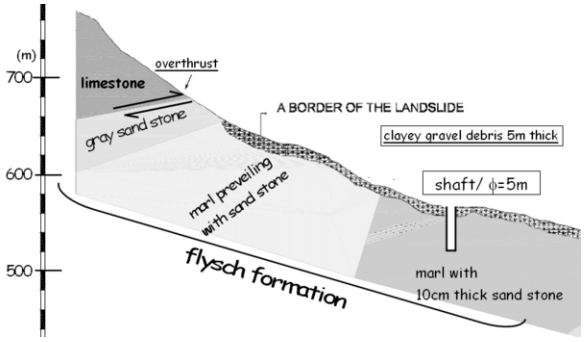

Fig.29 geological section of Slano blato sliding zone

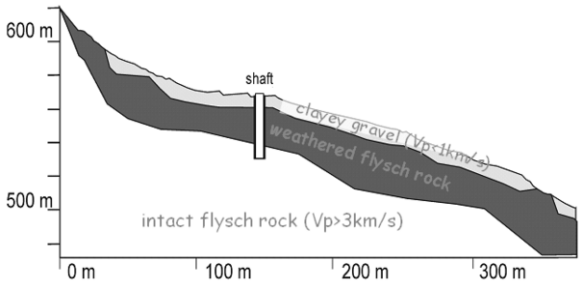

Fig.30 seismic refraction result

The result of seismic survey is shown in Fig.30. The thickness of this gravely layer is 3 to 11 m. Based upon seismic refraction survey, top sliding formation was found as Vp=1.0km/s and the intact Flysch rock as more than 3.0 km/s.
The geotechnical characteristics of clayey material in the sliding formation were studied. Natural water contents ranges about 14-27%. Plastic and Liquid limits are 15-20% and 45-50% respectively as shown in Fig.31. It may be understood that suction pressure less than 10kPa corresponds to the state of little shear strength of Liquid Limit.

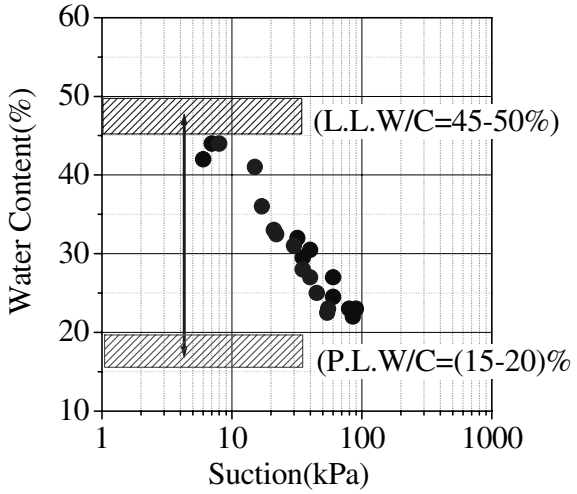

Fig.31 Water content and suction

In 2007, soil suction sensors were installed at the shallow depths in different zones. Fig.32 shows an example of the seasonal change of the suction as well as rainfall in 2008. The rainfall was shown as accumulative rainfall from the beginning of the year and 28days rainfall. The periods when the mass deformation prevailed at the upper zone with slope angle steeper than 23°are also shown in the figure.
The monitored suction decreases from 350kPa in January of dry season to 10kPa in May with rainfall of 200mm/28days.The mass sliding periods correspond to the very low suction that corresponds to water contents of liquid limit except the winter season that began from November.

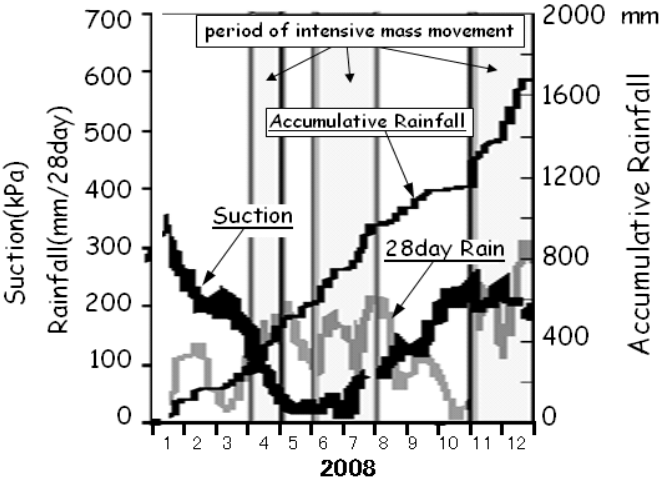

Fig.32 Change of suction and rainfall at point(ii)

It was clearly shown that the suction could be an observable index that is more appropriate to evaluate available shear strength than the rainfall itself.

3.8 *E Millis, S.W.Real-time Monitoring of Ground Movement and Groundwater Conditions associated with Landslides in Hong Kong HongKong*

Hong Kong has been developing mountain hilly area and resulted in manmade steep slope. It has been reported about 300 slope failures every year in Hong Kong that occurred during or after heavy rainfall. In 1977, Geotechnical Control Office(GCO) was established and worked to improve the slope stability control. The establishment of GCO and implementation of comprehensive Slope Safety System has resulted in a significant decrease of the fatalities from over 420 between 1948 and 1977 to about 50 since 1977 to present.
Whist significant improvement was achieved in slope safety management risk from man-made slopes, the Geotechnical Engineering Office (GCO was renamed as GEO in 1991) has continued to take a pro-active approach not only man-made but also natural slopes.
In 2005, GEO began to test the performance of various instruments and arranged pilot instrumentation schemes to set up a proto type realtime instrumentation networks at four study areas in Hong Kong as shown in Table-4 and Fig.33.
These four study areas have specific characters in terms of their slope instabilities.

Table-4 Four study sites of slope stability

	Site	Geology /Topology	Mechanism	Failure mode
1	Tsing Shan Foothills, NW New	decomposed Andesite	landslide by rainfall sliding surface 4-5m	slow creep 80mm/year 45000m3
2	Tung Chung Foothills, Lantau Island	collunium/saprolite	seasonal downward movement of loss of suction	slump 45mx10mx(2-3)m
3	Pa Mei, Lantau Island	high density failures in natural terrain	shallow open hillside typevarious type less than 100m3	10 sites, less than 100m3 incl brittle, shallow
4	Ching Cheung Road, Kowloon	cutslope with natural terrain	tanks and pipes for seepage	delayed failure after rainfall

Site 1.The slope at Tsing Shan Foothills is a typical landslide that was confirmed to move with a rate of about 80mm/year during 2002 to 2006.
Site 2 Slope at Tung Chung Foothills site composes of shallow 2-4m slump failure that might be reactivated by rainfall. The sliding surface is between the colluvium and saprolite boundary. The decrease of soil suction and high pore water during rainy storms is considered as main reason for the slope instability.

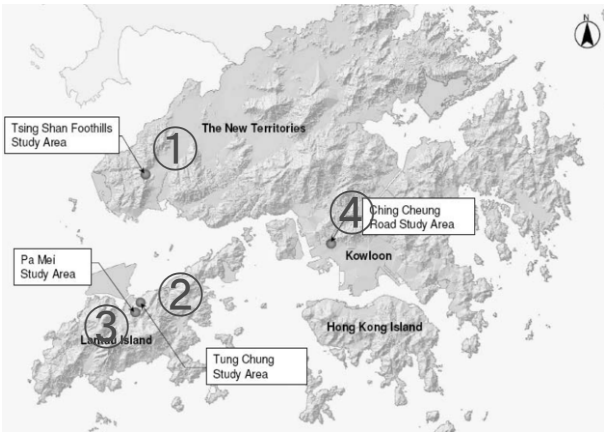

Fig.33 Four study sites for slope stability in Hong Kong

Site 3 Pa Mei site differs from the preceding sites. This site contains about 10 unstable slopes that locate at open hill slope. Each unstable slope is rather small scale of volume less than 100m3. Nearly all of the slopes appears to have failed in a brittle manner, with little or no obvious signs of distress.
Site 4 Ching Cheung Road is a cut slopes as well as a thin strip of natural terrain above.
The cut slope have been experienced several large slope failures. Most of them failed with some delays after heavy rainfall caused by “tank and pipe” of underground reservoir system.

Instrumentation for slope monitoring
Recent development of sensors and instrumentations has made possible to use realtime monitoring system with reasonable expense.
It was decided to adapt the following key items which will give benefit for slope engineering in Hong Kong area.
a) Surface deformation;
b) Sub-surface deformation;
c) Ground water levels at multiple points throughout the geological profile; .
d) soil suction and moisture contents; and
e) Other environmental factors such as rainfall / run off etc.

Monitoring of surface deformation
Three kinds of sensors system are adapted as follows,
1. Traditional type of vibrating wire displacement meter for surface crack gage.
2. Multi-point Tension and Rotation and Settlement System
3. Automated Differential Global Positioning System

Sub-surface deformation monitoring
In addition to the conventional method of inclinometer as well as in-place inclinometers system to obtain vertical displacement, Time Domain Reflectometry (TDR) was introduced to identify the sliding depth.

Hydro-geological monitoring
Rainfall and groundwater as well as soil matrix suction are monitored by such traditional sensors as automatic tipping bucket rain gauge, multi-level pore pressure meters, and Jet Filled Tensiometer.
New device of Time Domain Reflectometry was introduced to measure volumetric water content in the area to study.
The realtime monitoring system that is being developed in Hong Kong may take a lead in providing a new direction of slope engineering.

3.9 *Uchimura, T. et al., Development of low-cost early warning system of slope instability for civilian use Japan*

Uchimura et al. developed a simple and low cost early warning system against slope failure based upon MEMS sensors and wireless net working. Two MEMS sensors are used to measure tilt of slope and volumetric water. Experimental slope model with 1m and 3m high with a gradient of 2:1 of horizontal to vertical as shown in Fig.34 was tested under an artificial rainfall of 15mm/hour.

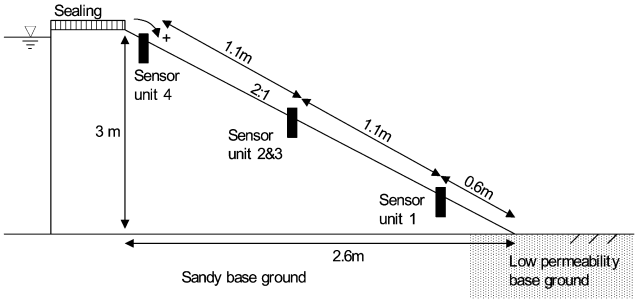

Fig.34 Experimental model slope

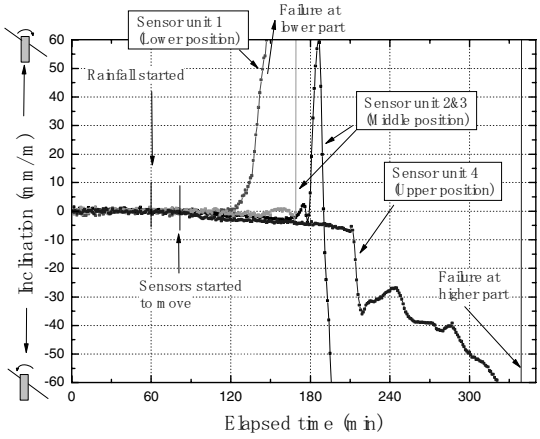

Fig.35 Response of Inclination sensor

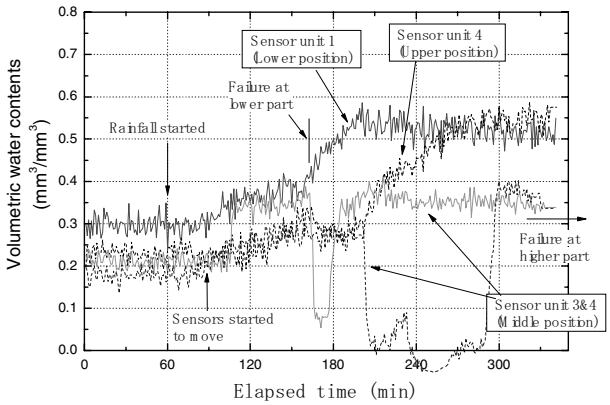

Fig.36 Response of Volumetric Water Sensor

Two sets of the sensors were installed within the slope at the depth of 20cm under the slope surface as shown in Fig.34. Responses of tilt and volume water are shown in Fig.35 and Fig.36. These sensors had responded some 30minutes before the slope began to fail. However, the responses of the tilt and water content before the failure depend upon case by case. It was difficult to use as some qualitative precursory signal at present. They have installed the same sensor system in a natural slope in Kobe and operated it for several months. The measure tiling values shows fluctuation in a range of 3mm/m that is 2-3times larger than those in laboratory test. Water volume contents responded sharp increase of the water contents. At present, the system works as expected to monitor the tilt and water contents, however, more efforts are needed to develop how to judge the signal as to predict slope failure.

3.10 *Riccio, M. Performance of a block-faced geogrid wall using fine-grained tropical soils Brazil*

Fine grained residual soils have been widely used as a backfill for reinforced soil wall construction in Brazil with success. Fine grained residual soils in the area are chemically weathered saprolite and show quite unique characteristics under compaction. The clay contents of the residual soil used as backfilled test were two different soils with clay contents (<2μm) of 42% with wL=38 and 49% and wP=16 and 20%. These tropical saprolite soils generally show good compaction and workability irrespective with water contents. An extensive instrumentation and monitoring were performed for real scaled geogrid system with block faced vertical wall to verify the mechanism and parameters for the design as shown in Fig.37.
Embankment height is 4.2m including concrete base of 0.2m thick at the bottom.

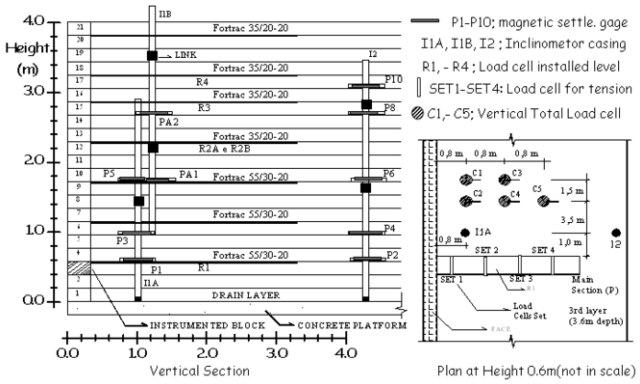

Fig.37 Retaining wall reinforced with Geogrid

One of the interesting points of the vertical retaining wall with geogrid is the distribution of the pressure against the wall. The tension forces were measured at four points along the 3m length of geogrid for the four heights of 0.6m, 2.4m, 3.0m and 3.4m.
The maximum tension of geogrid are shown in Fig.38 against height and noted as rather constant value.

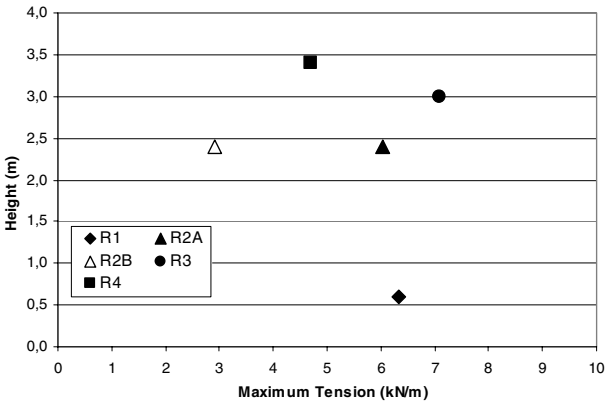

Fig.38 Maximum tension vs. Height

The tension force was measured during the compaction stage at four different points along the geo-grid at the height of 3.2m (R4 in Fig.37). In the middle of the horizontal axis of time, forces were recorded abrupt increase that was caused by tamping procedure. After the compaction, most of the load returns the initial values except t3.

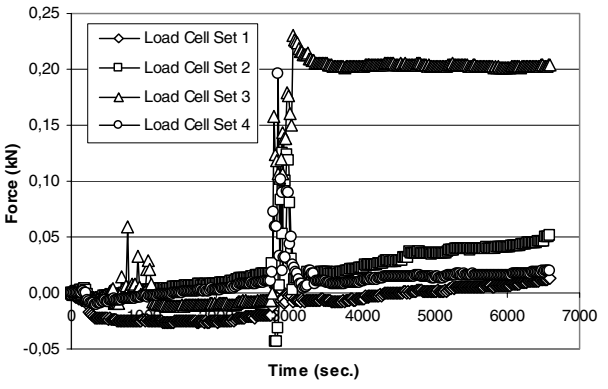

Fig.39 Change of Tension of Geogrid during compaction

The tension loads of the geogrid were compared with several methods of analysis and found to correspond well to Ehrich and Mitchell (1994).
The tendency of uniform distribution of the maximum tension in the reinforcement was due to compaction operations.

Compaction stress, soil cohesion, and soil stiffness should be considered to treat the geo-grid reinforcement.

3.11 *Hommels, A. Influence of the different types of measurements on the inverse modeling process of an road embankment, Netherlands*

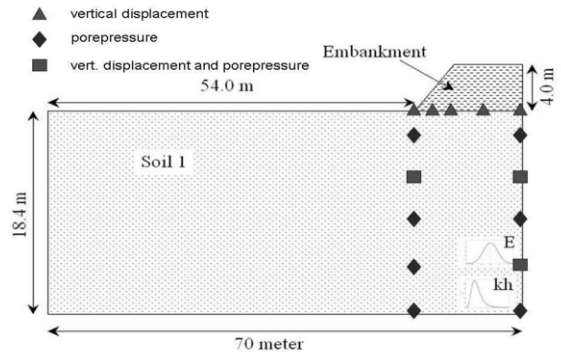

Fig. 40 Embankment model used for simulation

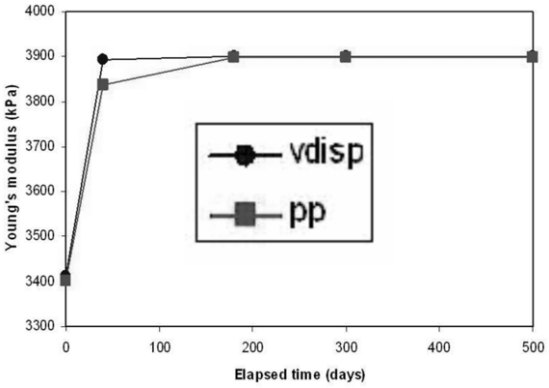

Fig.41 update process of Young's modulus E using measurements of the pore pressures (pp) or measurements of the vertical displacements (vdisp)

This paper presents a mathematical approach to feed monitored data to the computer and to improve the parameters based upon Ensemble Kalman filter(EKF). A mathematical simulation of an embankment on soft ground that is linear elasto-plastic Mohr Coulomb model was used for this case study. As the observation items, settlement and pore water pressure were selected and the model parameters to be identified were Young's modulus and permeability as shown in Fig.40.

Fig.41 shows the comparison of updating process of Young's modulus based upon the information of pore pressure data or settlement. The results showed that if settlement data is used to estimate permeability, it took longer time than by pore pressure data. The same tendency is found that pore pressure data resulted in faster to reach the right solution.

In general, there are different intensity of mutual effect among measuring item and characteristics of ground to be identified.

It should be noted that the most effective monitoring items should be considered according to the characteristics of the model, if the inverse modeling process is required effective.

4 CONCLUSIONS

The new technologies of instrumentations and sensors in geotechnical engineering are briefly reviewed. In the last decade, sensors have showed significant development. These various sensors based on MEMS consist of sensing part and data processing circuit. Technology of MEMS provides various sensors of smaller size, less expensive in price, and smaller power consumption.

Geochemical sensor is shown to provide the process of change of soil characteristics like leaching and may be used as precursory signal for slope instability. Magnetic sensor is also shown to provide simple and useful method to monitor stresses induced in steel. Monitoring stress of nut of earth anchor may provide easy and economical methods to test the integrity of the anchoring system.

TDR sensor becomes available based upon MEMS to measure volume water contents. Fiber optical sensors has been developed a new technology named BOTDR that provides continuous change of strains and temperatures along the optical cable.

Displacement sensing system based upon GPS provides accuracy of 2-5mm as relative displacement.

Wireless networking is a new trend of data logging in geotechnical engineering.

There are 11 papers that were presented in this TS-3 and grouped into several topics of sensors, observational method, slope instability, reinforced instability, and back analysis. Six papers are reports on sensor itself and/or some application of MEMS sensor.

The instrumentation in the geotechnical engineering is the bridge between theory and practice. The realtime monitoring used for natural hazard like the slope instability is the bridge between the engineers and citizens.

Most of the geotechnical engineering has been successful to evaluate the safety of construction based upon instrumentation.

However, we still need to advance basic mechanism and how to predict and with what kinds of sensors in the warning system against failure of natural slope.

REFERENCES

Akutagawa S. et al. (2008) New Evaluation method of PS-Anchor Force by Using Magnetic Sensor and Its Application in a Large Underground Powerhouse Cavern, Journal JSCE F., Vol.64, No.4, pp413-430, 2008.12(in Japanese)

Ehrlich, M. & Mitchell, J. K. 1994. Working Stress Design Method for Reinforced Soil Walls, Journal of Geot. Eng., Vol. 120, no. 4, pp. 625-645.

Iwasaki Y.,2008, Observation of CPT GPS at Kobe Laboratory, GRI report 2008, GRI

Nakano, M., Yamazaki, H., and Okuno, M., 2003, "The earthquake disaster prevention monitoring system using optical fiber technology," JSCE Journal of Earthquake Engineering, Vol.27, pp.1-4

Mohamad, H. 2008. Distributed Optical Fibre Strain Sensing of Geotechnical Structures. PhD thesis, University of Cambridge.

Mohamad, H., Bennett, P.J., Soga, K., Klar, A. & Pellow, A. 2007. Distributed Optical Fibre Strain Sensing in a Secant Piled Wall. Proceedings of the Seventh International Symposium on Field Measurements in Geomechanics (FMGM2007), ASCE Geotechnical Special Publication, No. 175.

Okuno, M., Kawano, M. and Hashimoto., T.,,2003, The Measurement System of the Foundation or a Structure Using the Optical Fiber Sensor, Proc. of the First China-Japan Geotechnical Symposium, Oct. 2003, Beijing, China

Sakai,H.(2001),Observation of Ground Displacement in Landslide by Monitoring Groundwater Composition, QR of RTRI, Vol.42, No.3

Sakai, H.(2009), prediction of Landslide a few months in advance of its occurrence with chemical sensors for groundwater composition observation, Proc. of the IS-Kyoto, Prediction and Simulation Methods for Geohazard

mitigation – Oka, Murakami, and Kimoto(eds), Taylor and Francis Group, London

Sasaki, Y., Unishi H., and Yahata T, (2004), Non-destructive Method for Stress Evaluation of Line pipes Using Magnetic Anisotropy Sensor, JFE Technical Report, No.3, p42-47(in Japanese)

Terzaghi K., and Peck R.B., (1967), Soil Mechanics in Engineering Practice, 2nd Edition, John Wiley & Sons, Inc.

Terzaghi K., Peck R.B., and Mesri G.(1996), Soil Mechanics in Engineering Practice, 3rd Edition, John Wiley & Sons, Inc.